ADVANCED MATERIALS INTERFACES
Open Access
www.advmatinterfaces.de

Beyond Fertilizers: NH_4ZnPO_4 for the Reversible Chemical Storage of Ammonia

Takahiro Kozawa, Tai Hashiba, Kayo Fukuyama, Hiroya Abe, Shu Morita, Minoru Osada, and Makio Naito*

Enhancing NH_3 as a carbon-free energy carrier of H_2 and next-generation fuel is a promising approach for a sustainable society. Chemically storing NH_3 molecules in crystal structures offers better selectivity and reusability than storage in traditional porous materials based on physicochemical adsorption; however, designing materials that can be reversibly stored in structural gaps is still a significant challenge. Herein, the use of NH_4ZnPO_4, which is previously used as a fertilizer, is proposed as an NH_3 uptake material through a chemical storage mechanism. The NH_4ZnPO_4 particles synthesized by a wet mechanochemical method with monoclinic and hexagonal crystal structures can incorporate NH_3 molecules and directly transform them into $NH_4Zn(NH_3)PO_4$ without producing byproducts. The chemical storage mechanism depends on the particle morphology; therefore, the uptake amount per surface area surpasses that of porous materials. NH_4ZnPO_4 exhibited excellent cycling performance due to its reusability, which is regenerated by releasing NH_3 from $NH_4Zn(NH_3)PO_4$ when heated in air at ≈100 °C. Taking inspiration from previously used and familiar fertilizers further extends this new area of innovative materials that can be used for the reversible storage of low-molecular-weight gases.

1. Introduction

Ammonia (NH_3) is a crucial raw material for various human activities, such as the production of fertilizers, chemical fibers, rubber, and resins. In the 21st century, the demand for a carbon-free energy carrier of H_2 has increased because H_2 gas can replace fossil fuels for thermal power generation due to its secure transport and storage and lack of CO_2 emissions during combustion.[1–3] Utilizing NH_3 offers advantages in reducing the cost of H_2 production and CO_2 emissions.[4] However, the intense odor and formation of ammonium salts within the atmosphere that cause PM2.5 remain fundamental issues that threaten public health.[5] Additionally, the NH_3 residue during H_2 production degrades the catalytic performance in applications such as fuel cells and biogas reforming.[6,7] Therefore, the search for and design of innovative materials suitable for the highly efficient capture and separation of NH_3 are closely related to constructing safe and sustainable societies.

In general, porous materials are employed for NH_3 uptake through physicochemical adsorption. Previously, inorganic materials such as activated carbon and zeolites have attracted attention as NH_3 uptake materials.[8,9] Nevertheless, they face technical challenges regarding pore structure control, reusability, and NH_3 gas selectivity. To address these challenges, metal–organic frameworks (MOFs) have recently emerged, in which the size of nanocages that capture NH_3 molecules can be tuned by altering the organic ligands and central metal ions.[10–16] The NH_3 molecules chemisorb strongly within the MOF structure but can also desorb upon heating.[17,18] Although this reversible and efficient uptake process is appealing, the high cost and complex synthesis of MOFs hinder their practical application.

As an alternative NH_3 uptake method to physicochemical adsorption, a chemical storage mechanism has been demonstrated in a lead-based organic–inorganic iodide perovskite.[19] When reacted with NH_3 vapor containing H_2O, the 1D columnar perovskite undergoes phase separation into a product with a 2D layered structure. The intermediate phase reacts with NH_3 to form two nitrogen compounds, which are chemically stored on the layered product. Although this approach shows high selectivity due to the direct reaction with NH_3, the dynamic structural transformation involving phase separation raises concerns about reversibility and structural stability during NH_3 uptake. As demonstrated by hydrogen storage alloys that change only the crystalline phase by

T. Kozawa, T. Hashiba, K. Fukuyama, H. Abe, M. Naito
Joining and Welding Research Institute
Osaka University
Osaka 567-0047, Japan
E-mail: kozawa.takahiro.jwri@osaka-u.ac.jp
S. Morita, M. Osada
Institute of Materials and Systems for Sustainability (IMaSS) and Department of Chemistry
Nagoya University
Nagoya 464–8601, Japan
The ORCID identification number(s) for the author(s) of this article can be found under https://doi.org/10.1002/admi.202400729

DOI: 10.1002/admi.202400729

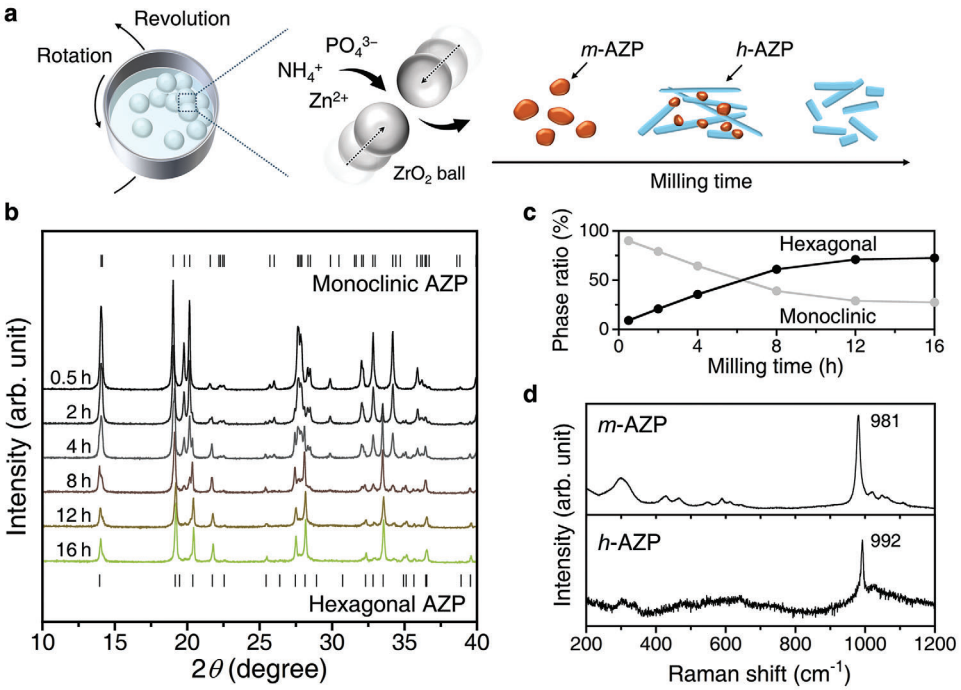

Figure 1. a) Schematic illustration of AZP particles obtained through the wet mechanochemical method using a planetary ball mill. b) XRD patterns of the products obtained by milling with ϕ5 mm balls. The diffraction peak positions for the monoclinic (*m*-AZP) and hexagonal (*h*-AZP) phases were added based on each ICDD database (*m*-AZP: 01-088-1126; *h*-AZP: 01-089-6315). c) Monoclinic and hexagonal phase ratio versus milling time. d) Raman spectra of *m*-AZP and *h*-AZP.

incorporating H_2 into the gaps in the structure,[20,21] a chemical storage mechanism that can take up NH_3 without dynamic phase separation should expand the possibility of exploring new materials.

Herein, we present the first evidence that agricultural fertilizers can be chemical storage materials for NH_3 without dynamic phase separation. Fertilizers that already immobilize NH_4^+ ions as a nitrogen source would have a high affinity for NH_3 and could further incorporate it within the crystal structure, similar to hydrogen storage alloys. However, to date, no fertilizer-inspired chemical storage materials have been developed. This work uses ammonium zinc phosphate (NH_4ZnPO_4, AZP), a previously used fertilizer,[22] as a novel NH_3 uptake material for allowing only a chemical phase change to $NH_4Zn(NH_3)PO_4$ (AZAP). With the advent of long-used agricultural fertilizers for chemical storage, the design guidelines for selective NH_3 uptake materials are at a significant turning point.

2. Results and Discussion

2.1. Synthesis and Characterization of AZP

The AZP powder was synthesized through a wet mechanochemical route in water with a planetary ball mill.[23,24] The wet milling of $Zn_4CO_3(OH)_6{\cdot}H_2O$ and $NH_4H_2PO_4$ produced monoclinic AZP (*m*-AZP) and hexagonal AZP (*h*-AZP) phases with increasing milling time (**Figure 1a**). The X-ray diffraction (XRD) pattern of the product after 0.5 h shows the formation of *m*-AZP and no residues of the raw materials (Figure 1b). Unlike other ammonium metal phosphates ($NH_4MPO_4{\cdot}xH_2O$, M = transition metal), AZP precipitates as an anhydride.[25] With increasing milling time, *h*-AZP appears after the formation of *m*-AZP. Although the XRD peaks of both phases are similar, the characteristic peaks at $2\theta = 21.7°$, 28.1°, 33.5°, and 39.5° distinguish the *h*-AZP phase. Eventually, *h*-AZP can be obtained after milling for 16 h. According to quantitative analysis based on the obtained XRD pattern, the hexagonal ratio reaches 73% (Figure 1c). Raman spectroscopic measurements revealed that *h*-AZP is sensitive to laser excitation and is significantly noisier than *m*-AZP (Figure 1d). The detected bands, derived from PO_4 tetrahedra, can be attributed to the following:[26,27] P–O symmetric stretching (ν_1) at ≈980–990 cm^{-1}, P–O antisymmetric stretching (ν_3) at ≈1000–1100 cm^{-1}, O–P–O symmetric bending (ν_2) at ≈250–500 cm^{-1}, and O–P–O antisymmetric bending (ν_4) at ≈550–650 cm^{-1}. The ν_1 mode position shifts to higher wavenumbers in *h*-AZP compared to that in *m*-AZP.[28]

The synthesized AZP particles showed shape anisotropy despite the milling process. The *m*-AZP particles obtained after 0.5 h were irregularly shaped nanoparticles with a size range of 50–200 nm (**Figure 2a**). In contrast, the product after 4 h of milling consisted of micron-sized particles that exceeded 5 µm in size and grew in the 1D direction (Figure 2b). Transmission electron microscopy (TEM) images show that some particles have an internal straw morphology (Figure 2c). The wall thickness and inner diameter are ≈85 nm and 150–200 nm, respectively. Scanning electron microscopy (SEM) images of the fracture surfaces confirmed the presence of micron-sized particles with a straw-like morphology (Figure S1, Supporting Information). Notably, during TEM, the AZP particles were

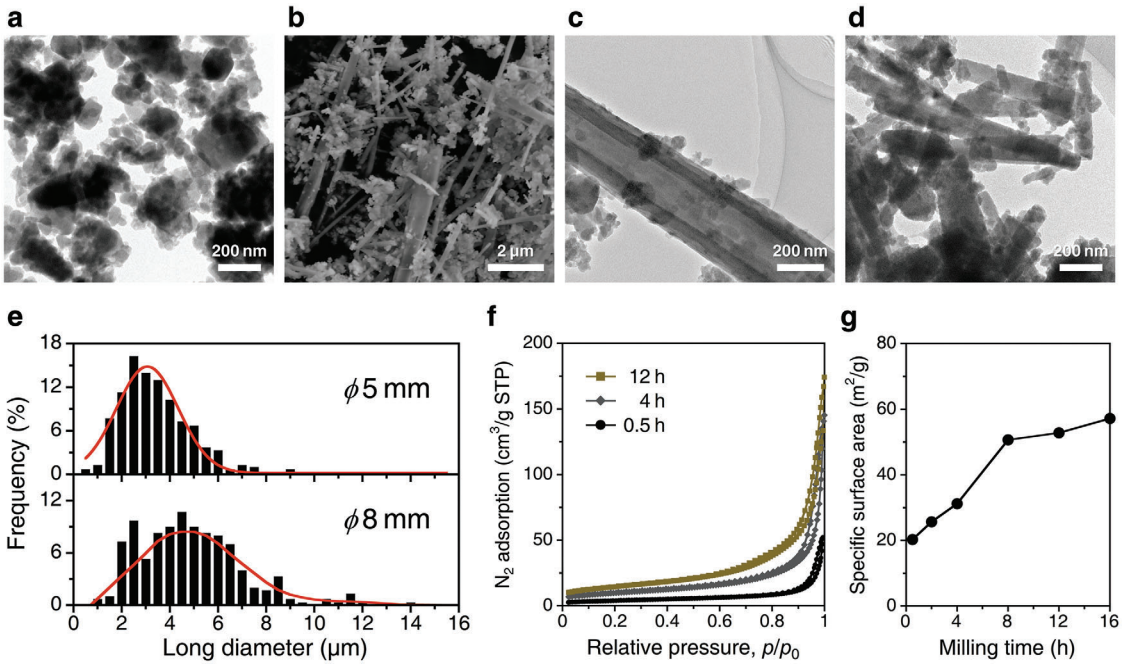

Figure 2. a–d) TEM and SEM images of AZP particles after milling for (a) 0.5 h, (b,c) 4 g, and (d) 12 h. e) The longitudinal size distribution of 1D-grown AZP particles after milling for 4 h. f) N_2 adsorption/desorption isotherms. g) Specific surface area of the AZP powders.

sensitive to electron beams, and prolonged irradiation or high irradiation energies caused their decomposition (Figure S2, Supporting Information). In this study, the energy of the electron beam used to irradiate the samples was suppressed by reducing the spot size. In wet mechanochemical synthesis, extra milling energy is employed to pulverize particles once their crystal growth is complete. The 1D-grown AZP particles larger than 5 μm were ground down to ≈500 nm (Figure 2d).

In wet mechanochemical synthesis, the ball size affects the crystalline phases and particle size of AZP powders. Increasing the ball size results in longer particle growth in the 1D direction (Figure 2e). This is due to the larger space between the balls, which allows crystal growth. Conversely, decreasing the ball size can promote the formation of *h*-AZP in a shorter time (Figure S3, Supporting Information). Particle synthesis through wet mechanochemical reactions is strongly related to the collision energy of the ball media, and small balls with greater collision frequencies can promote the reaction more efficiently.[29]

Unsimilar to the nanocages in MOFs, the synthesized AZP particles have nearly no pores. A detailed evaluation of the pore structure, which is generally required for gas adsorption in porous materials, was conducted through N_2 adsorption/desorption measurements (Figure 2f). The hysteresis region appears in the relative pressure range of 0.9 to 1, indicating that the synthesized AZP contains few nanopores below the mesopore size (Figure S4, Supporting Information); the straw-like macropores shown in Figure 2c do not affect the N_2 adsorption/desorption measurements. The specific surface area (S_w) of the AZP powders increased with milling time (Figure 2g). Therefore, the characteristic properties of the synthesized AZP powder are attributed to the particle shape and size.

2.2. Formation Mechanism of AZP Particles

The formation of AZP proceeds through the dissolution–precipitation reaction of raw materials triggered by the collision of ball media. $NH_4H_2PO_4$ is soluble in water, while $Zn_4CO_3(OH)_6{\cdot}H_2O$ has a low solubility (1 mg 100 mL^{-1}). However, the reaction solution with dissolved $NH_4H_2PO_4$ is weakly acidic (pH ≈4.8), so $Zn_4CO_3(OH)_6{\cdot}H_2O$ can gradually dissolve in the solution during milling. In addition, planetary ball milling reduces the particle size of the raw materials to promote dissolution. The collision of ball media generates local and instantaneous high-temperature and high-pressure zones that trigger solubility changes, resulting in the nucleation of AZP. From a combined analysis of the experimental reaction rates and the simulated ball motion, our group previously found that ball collisions in the normal direction contribute to nucleation,[29] as depicted in Figure 1a. When using soluble zinc sources, such as $ZnCl_2$ and $Zn(CH_3COO)_2{\cdot}2H_2O$, $Zn_3(PO_4)_2$ hydrates are formed by a preferential condensation reaction between PO_4^{3-} ions (Figure S5, Supporting Information). Therefore, the solubility of raw materials plays a crucial role in particle synthesis via wet mechanochemical reactions.

Owing to the dissolution–precipitation reaction, the crystal growth in the 1D direction of *h*-AZP is attributed to its crystal structure.[24,30] For the crystal structure of *h*-AZP, the PO_4 and ZnO_4 tetrahedra are arranged in a zigzag pattern along the *c*-axis sharing a vertex.[31] This results in preferential crystal growth in the *c*-axis direction, producing needle- or rod-like particles. The difference in the growth rate of each crystal plane produces straw-like particles,[32,33] as shown in Figure 2c. As in the general solution method, shape-anisotropic particles can be formed through the dissolution–precipitation reaction in the wet

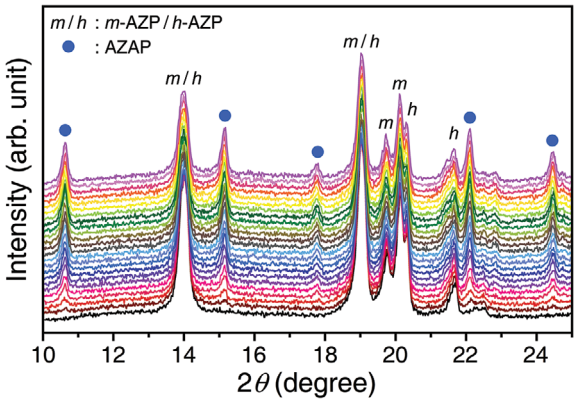

Figure 3. In situ XRD patterns for the transformation of AZP-4 to AZAP upon exposure to the saturated vapor of a 28% NH_3 solution at 25 °C.

mechanochemical method. The particle size depends on the processing time and ball diameter, as crystal growth is limited by the space between ball media. In terms of the relative stability of *m*-AZP and *h*-AZP, the latter is slightly more stable.[28,34] The monoclinic phase, which is a dense structure, can be stable at high temperatures and pressures if both crystalline phases have an equilibrium stability field.[34] Therefore, in wet mechanochemical reactions, where local nonequilibrium conditions are generated, the formation of *m*-AZP would be preferential in the early stages. However, experimental analysis has not been conducted, and the phase stability is debatable.

2.3. NH_3 Uptake Properties of AZP

The AZP particles can incorporate NH_3 molecules within their crystal structure without dynamic phase separation and transform into AZAP. In situ XRD measurements verified this transformation process via a solid–gas reaction (**Figure 3**). The AZP powder containing monoclinic and hexagonal phases and a 28% NH_3 solution were placed in an airtight domed holder to avoid direct contact. Within 30 min, the AZAP phase appeared. The intensity of the diffraction peaks of the AZAP phase increased with increasing exposure time. The changes in the diffraction peak intensities attributed to each of the two crystalline phases in the AZP and AZAP samples indicate that the amounts of the monoclinic and hexagonal phases decrease with the formation of AZAP (Figure S6, Supporting Information). AZP undergoes a phase change to AZAP regardless of its crystal structure. In addition, no byproducts are generated. This is evidence of the direct storage of NH_3 molecules in the structure.

The uptake performance was evaluated from exposure tests in the saturated vapor of a 28% NH_3 solution at 25 °C in a sealed container. The AZP samples evaluated were powders synthesized with ϕ5 mm balls for 0.5, 4, and 12 h, denoted as AZP-05, AZP-4, and AZP-12, respectively. After 48 h of exposure, the NH_3 uptake per weight ranged from 8.2 to 10.6 mmol g^{-1} (**Figure** 4a). Since the theoretical storage capacity of AZP for incorporating one NH_3 molecule is 5.6 mmol g^{-1}, these results suggest that physical adsorption on the product surface, including H_2O molecules in the vapor, also occurs. A comparison of the properties within the AZP samples shows that AZP-05, which consists of irregularly shaped, fine monoclinic particles, is already saturated at the initial exposure stage up to 4 h. Meanwhile, the NH_3 uptake increases asymptotically with the exposure time for 1D-grown AZP-4 and AZP-12. Furthermore, the uptake properties of activated carbon and zeolite, which are typical inorganic porous materials based on a physical adsorption mechanism, were also investigated. Zeolite, like AZP-05, reaches saturated adsorption (≈8.1 mmol g^{-1}) in the early stage, while activated carbon has more than twice the storage capacity (23.6 mmol g^{-1}) of AZP. This result is due to the large S_w of activated carbon; the S_w of the activated carbon and zeolite used are 1071 and 359 m^2 g^{-1}, respectively (Figure S7, Supporting Information). Therefore, we compared the NH_3 uptake per surface area (Figure 4b). These results show that AZP has a significantly greater uptake than inorganic porous materials. In addition, the AZP samples with smaller S_w values incorporated NH_3 in a shorter time, suggesting that the NH_3 uptake performance of AZP depends on the particle size and shape rather than the pore structure.

AZP underwent a complete phase change to AZAP after 48 h of exposure to NH_3 vapor (Figure 4c). The AZAP phase transformed from AZP-4 is consistent with the simulation pattern of AZAP.[35] Furthermore, the Raman spectrum reveals that the ν_1 mode for PO_4^{3-} shifted to a lower wavenumber than that of both AZP phases (Figure 4d). The overall spectrum is broad and similar to that of *h*-AZP but resembles that of *m*-AZP below 600 cm^{-1}. The significant transformation in the particle morphology occurs after the phase change. AZAP particles transformed from 1D-grown AZP-4 exhibited a plate-like morphology of ≈1 µm (Figure 4e). This is due to the rearrangement of the crystal structure upon NH_3 uptake, resulting in fragmentation of the particles and subsequent crystal growth. The crystal growth may be influenced by H_2O vapor in the exposed atmosphere. According to this shape change, AZP-05, an irregular and isotropic nanoparticle, suppresses the effects of the fragmentation step and permits the phase change to AZAP during the early stage (Figure 4c,d). The chemical storage mechanism of NH_3 molecules from the particle surface is independent of the pore structure, and the particle size and shape affect the uptake performance.

The NH_3 molecules enter channels in the crystal framework and induce a phase change from 3D to 1D structures. The *m*-AZP phase, which has an ABW-type zeolite structure, possesses channels with eight-membered rings of ZrO_4 and PO_4 tetrahedra,[36,37] while the *h*-AZP phase consists of channels with six-membered rings (**Figure 5**). These channels in the 3D frameworks contain NH_4^+ ions. In contrast, AZAP has a 1D ladder structure with a four-membered ring as the basic unit consisting of $ZnO_3(NH_3)$ and PO_4 tetrahedra linked together, with NH_4^+ ions located in the gaps between the frameworks.[35] The packing structure surrounding the PO_4 tetrahedron accounts for the varying peak position of the ν_1 mode in the Raman spectrum. The NH_3 molecules break the Zn–O–P bridges by coordinating with the Zn ions of the readily accessible AZP crystal framework, causing structural rearrangement. Zinc phosphates, in which both Zn and P atoms adopt tetrahedral coordination, build 0D, 1D, 2D, and 3D structures from combinations of basic four-membered ring units.[38,39] In general, the rearrangement of these basic units transforms zinc phosphates from

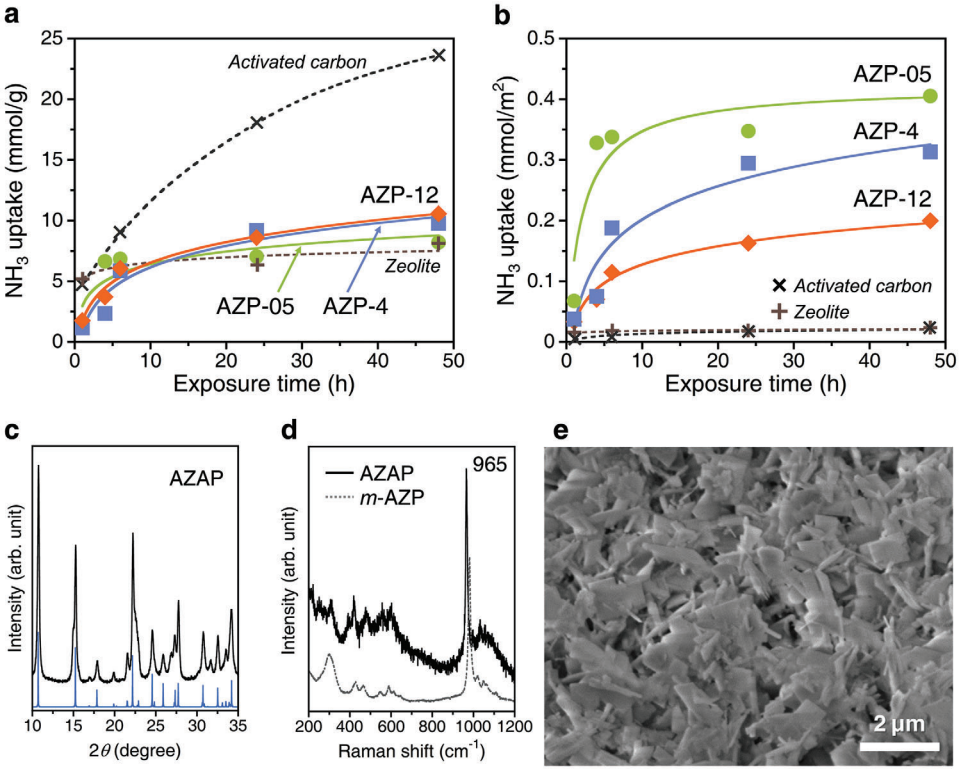

Figure 4. a) NH_3 uptake per weight for AZP and inorganic porous materials. b) NH_3 uptake per surface area recalculated from (a). c) XRD pattern, d) Raman spectrum, and e) SEM image of AZAP transformed from AZP-4 by exposure to NH_3 vapor for 48 h.

low- to high-dimensional structures. Moreover, AZAP with a 1D structure was discovered in the study of the transformation of 2D layers to 3D structures.[35] The 2D $NH_4Zn_2(PO_4)(HPO_4)$ layered compound transforms to 1D AZAP under NH_3 vapor. This phase change was made possible by the cleavage of basic units within the $[Zn_2(PO_4)(HPO_4)]^-$ anionic layer. However, the direct transformation from a 3D to 1D structure by incorporating NH_3 molecules has never been reported. Although releasing NH_3 molecules from AZAP with an endothermic reaction has been indicated by Amghouz et al.,[35] we found that this reverse reaction, i.e., an exothermic one, is kinetically possible. Consequently, the chemical storage mechanism is achieved by utilizing gaps in the crystal structure and structural rearrangement without producing byproducts. There may be other candidate materials that can chemically incorporate NH_3 molecules among transition metal phosphates with various crystal frameworks.[40]

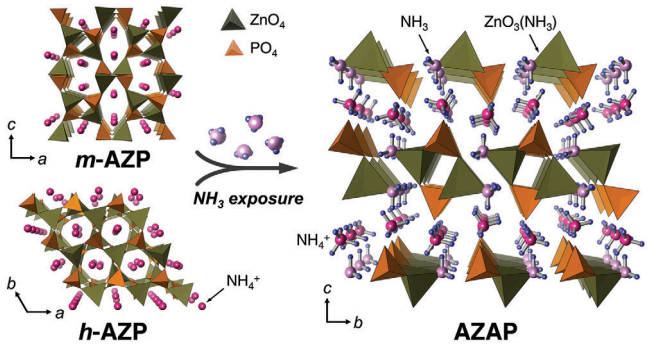

Figure 5. Illustration of the chemical storage mechanism for NH_3 in AZP. Crystal structures were drawn using VESTA software.[37]

2.4. NH_3 Release from AZAP and Cycle Performance

The NH_3 molecules incorporated as AZAP are readily released by low-temperature heating in air and regenerated to AZP. We investigated NH_3 release behavior by heating AZAP, which was transformed by exposing AZP-4 to saturated vapor from a 28% NH_3 solution at 25 °C for 24 h (**Figure 6a**). Under heating conditions at 25 and 60 °C in air, the released amount leveled off after 24 h, exhibiting 3.5 and 5.5 mmol g^{-1}, respectively. The average NH_3 uptake of AZP-4 was 9.2 mmol g^{-1}, and the physical adsorption deducted from the theoretical amount was 3.6 mmol g^{-1}. Therefore, physisorbed NH_3 can be desorbed at 25 °C, and release begins within the AZAP structure upon heating at 60 °C. Increasing the temperature to 100 °C further accelerated the release. The release of 9.8 mmol g^{-1}, equivalent to the uptake amount, was obtained after 48 h. The XRD pattern of the product after heating at 120 °C for 24 h revealed regeneration of monoclinic AZP (Figure 6b). Once AZP-4, a mixture of monoclinic and hexagonal phases, transforms to AZAP, only the monoclinic phase is formed during regeneration to AZP. The regenerated AZP particles are plate-like particles that are slightly refined while reflecting the shape of AZAP (Figure 6c). The ability to regulate the release of NH_3, one of the desired properties, reflects the sustained-release properties exhibited in fertilizer applications. If

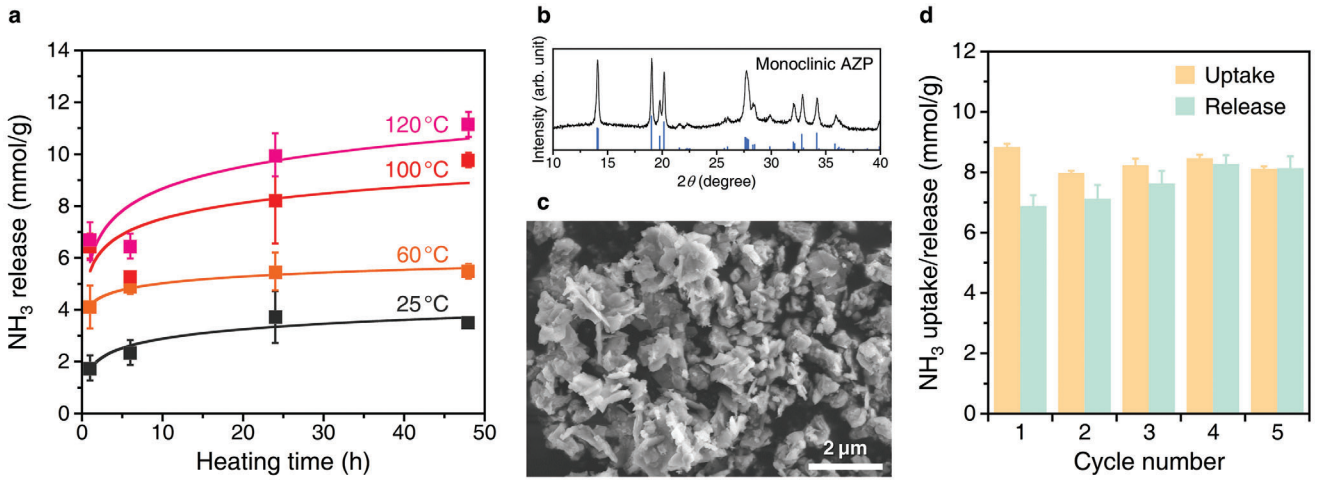

Figure 6. a) Atmospheric heating with AZAP transformed by exposing AZP-4 to the saturated vapor of a 28% NH_3 solution at 25 °C for 24 h. b) XRD pattern and c) SEM image of regenerated AZP after heating at 120 °C for 24 h. d) Cycle performance of NH_3 uptake and release using AZP-4; uptake at 25 °C and release at 100 °C for 24 h each.

strongly chemically bonded within the structure, acid washing or heating processes above 150 °C are required.[10,16,17] By reducing the pressure, the heating temperature for the release of NH_3 is lowered.[12,19] Compared to conventional uptake materials, NH_3 molecules in AZAP are weakly bonded by coordination bonds to Zn^{2+} ions. Thus, the fact that NH_3 can be readily released by heating at a low temperature of ≈100 °C under atmospheric pressure leads to lower energy consumption for reusability.

On the other hand, temperature restrictions exist for the use of AZAP and AZP. Continued heating of AZAP at 120 °C resulted in further weight loss, i.e., the release of NH_3 associated with the partial decomposition of AZP. According to the thermal analysis, AZP can withstand temperatures up to 200 °C but gradually decomposes by releasing NH_3 above that temperature (Figure S8, Supporting Information). During the regeneration process from AZAP to AZP, the binding force of NH_4^+ ions within the structure decreases. Consequently, decomposition occurs after prolonged holding, even at 120 °C. These results suggest that 100 °C is sufficient for NH_3 release from AZAP.

We further evaluated the cycling performance of AZP as an NH_3 uptake material (Figure 6d). By increasing the number of cycles, the amount of NH_3 released approached the uptake amount, and the efficiency was almost 100% by the fifth cycle. Since particle shape changes associated with uptake and release are completed only in the initial stage, these NH_3 amounts are nearly constant. A chemical storage mechanism without dynamic phase separation or byproduct formation can provide stable cycling performance. The ability to readily release this material increases its practical advantage.

3. Conclusion

In summary, we synthesized AZP particles, which were previously used as a fertilizer, as a new material for NH_3 uptake. Using a planetary ball mill, a wet mechanochemical technique produced monoclinic and hexagonal anisotropic AZP particles via a dissolution–precipitation reaction. The resultant AZP particles incorporated NH_3 molecules into their crystal structure, resulting in a phase change to AZAP. The chemical storage mechanism involving this phase change was a reversible reaction that allowed NH_3 release under operable atmospheric heating conditions below 100 °C. Compared to conventional inorganic porous materials, AZP exhibited a much greater NH_3 uptake capacity per surface area and superior cycling performance. The phase change process between AZP and AZAP is a reversible kinetic reaction; therefore, the reaction rate depends on the relative pressure of NH_3 and the particle morphology. Although this study was conducted in a saturated vapor atmosphere of a 28% NH_3 solution at 25 °C, the reaction would be completed in a shorter time in a high-pressure NH_3 gas atmosphere. In addition, the phase change from the particle surface allows the response to be accelerated by fine particles with a large surface area. By focusing on fertilizers, which are well-known materials that have a high affinity for nitrogen compounds, a new functionality of NH_3 uptake was discovered. A chemical storage mechanism within the crystal structure utilizing a reversible phase change would further expand the candidate materials for capturing and separating low-molecular-weight gases such as H_2, NH_3, and CO_2.

4. Experimental Section

Chemicals and Materials: Ammonium dihydrogenphosphate ($NH_4H_2PO_4$, 99.0%), zinc carbonate basic ($Zn_4CO_3(OH)_6{\cdot}H_2O$, 69–74% as ZnO), zinc chloride ($ZnCl_2$, 98.0%), zinc acetate dihydrate ($Zn(CH_3COO)_2{\cdot}2H_2O$, 99.9%), activated carbon (powder), zeolite (molecular sieves, 13X), and ammonia solution (28 mass% in water) were obtained from commercial sources (FUJIFILM Wako Pure Chemical, Japan) and directly used without further purification. Pure water was used in all experiments.

Wet Mechanochemical Synthesis of AZP: Typically, water (20 mL) and Y_2O_3-stabilized ZrO_2 balls (100 g) 5 mm in diameter were placed in a stainless-steel vessel (170 cm^3). Then, $NH_4H_2PO_4$ and $Zn_4CO_3(OH)_6{\cdot}H_2O$ with a PO_4/Zn molar ratio of 1.2 (total of 3 g) were added to this vessel. The vessel was sealed and fixed in a planetary ball milling apparatus (High-G BX254E, Kurimoto, Japan). The milling was conducted for up to 16 h under a centrifugal acceleration of 150 G. The rotation and revolution were in the same direction, and the speed ratio of

rotation/revolution was a constant value of 0.497. After milling, the suspension was separated from the balls with a screen. The solid product was collected using centrifugation, washed with water and ethanol, and dried in an oven at 100 °C.

Evaluation of NH_3 Uptake Performance: Sample NH_3 uptake performance was evaluated by determining the weight change after exposure to the saturated vapor of a 28% NH_3 solution at 25 °C. A borosilicate glass test tube (ϕ12 × 75 mm) containing AZP powder (0.1 g) was placed in a polystyrene conical tube (50 cm^3). Then, 28% NH_3 solution (5 mL) was added to the conical tube without contacting the AZP powder. After being sealed, the conical tube was placed in an incubator at 25 °C. Exposure to NH_3 saturated vapor ranged from 1 to 48 h. For comparison, the same experiments were conducted with general inorganic porous materials, such as activated carbon and zeolite.

The release of NH_3 from AZAP was evaluated by heating under ambient atmospheric pressure. The AZAP powder, obtained by NH_3 vapor exposure for 24 h, was kept in an oven from 25 to 120 °C for up to 48 h in an open system. The amount of NH_3 released was estimated from the weight change. The cycling test was performed by repeating the NH_3 vapor exposure at 25 °C and the heat treatment at 100 °C for 24 h each. All NH_3 uptake and release experiments were performed three times for each sample.

Characterization of Materials: The crystalline phases of the obtained products were characterized by powder XRD (D2 PHASER, Bruker AXS, Germany) using Cu Kα radiation at 30 kV and 10 mA. Diffraction patterns were acquired in steps of 0.02° (2θ) with a counting time of 0.5 s/step. Simplified in situ XRD measurements during the NH_3 uptake process for AZP were performed using an airtight domed holder (Bruker AXS). AZP powder and a small amount of 28% NH_3 solution were placed in the center and edges of the holder, respectively, to avoid direct contact. Interval XRD measurements were started immediately after attaching the airtight dome. The particle morphologies were examined by SEM (SU-70, Hitachi, Japan) and TEM (JEM-2100F, JEOL, Japan). Raman spectra were acquired using a micro-Raman system (LabRAM HR-800, Horiba Jobin-Yvon, France) with a 532 nm excitation laser. The specific surface areas of the samples and their pore size distributions were estimated from the results of N_2 adsorption/desorption measurements (3Flex, Micromeritics, USA) using the Brunauer–Emmett–Teller (BET) and Barrett–Joyner–Halenda (BJH) methods, respectively. Before each measurement, the pre-outgassed sample was further treated under vacuum for 3 h at 60 and 120 °C for the AZP and inorganic porous materials, respectively. Thermal analysis was performed using a thermogravimetric differential thermal analyzer (TG-DTA; TG-DTA8122S, Rigaku, Japan) in the air with a flow rate of 200 mL min^{-1}.

Supporting Information

Supporting Information is available from the Wiley Online Library or from the author.

Acknowledgements

The authors acknowledge the financial support from the Grant-in-Aid for Scientific Research KAKENHI (24K01180, 24K21675) and the Cooperative Research Project of Design & Engineering by Joint Inverse Innovation for Materials Architecture (DEJI^{2}MA) of the Ministry of Education, Culture, Sports, Science and Technology (MEXT). T.K. was supported by the JWRI Young Researcher Grant Program. The authors thank Takeshi Murakami for the TEM observations.

Conflict of Interest

The authors declare no conflict of interest.

Author Contributions

T.K. and T.H. conceived and developed the idea and planned the experiments. T.K., T.H., and K.F. performed the particle synthesis, characterization, and NH_3 uptake. S.M. and M.O. contributed to the Raman spectroscopy measurements. T.K. and M.N. managed the research. H.A. provided constructive suggestions. T.K. and H.A. prepared the manuscript. All authors approved the submission.

Data Availability Statement

The data that support the findings of this study are available from the corresponding author upon reasonable request.

Keywords

ammonia, ammonium zinc phosphate, chemical storage, fertilizer, reversible phase change

Received: September 5, 2024
Revised: November 21, 2024
Published online:

[1] A. Klerke, C. H. Christensen, J. K. Nørskov, T. Vegge, *J. Mater. Chem* **2008**, *18*, 2304.
[2] D. R. MacFarlane, P. V. Cherepanov, J. Choi, B. H. R. Suryanto, R. Y. Hodgetts, J. M. Bakker, F. M. Ferrero Vallana, A. N. Simonov, *Joule* **2020**, *4*, 1186.
[3] A. Valera-Medina, H. Xiao, M. Owen-Jones, W. I. F. David, P. J. Bowen, *Prog. Energy Combust. Sci.* **2018**, *69*, 63.
[4] S. Wu, N. Salmon, M. M.-J. Li, R. Bañares-Alcántara, S. C. E. Tsang, *ACS Energy Lett.* **2022**, *7*, 1021.
[5] B. Gu, L. Zhang, R. V. Dingenen, M. Vieno, H. J. M. Van Grinsven, X. Zhang, S. Zhang, Y. Chen, S. Wang, C. Ren, S. Rao, M. Holland, W. Winiwarter, D. Chen, J. Xu, M. A. Sutton, *Science* **2021**, *374*, 758.
[6] F. A. Uribe, S. Gottesfeld, T. A. Zawodzinski, *J. Electrochem. Soc.* **2002**, *149*, A293.
[7] W. Yin, N. Guilhaume, Y. Schuurman, *Chem. Eng. J.* **2020**, *398*, 125534.
[8] M. Gonçalves, L. Sánchez-García, E. de Oliveira Jardim, J. Silvestre-Albero, F. Rodríguez-Reinoso, *Environ. Sci. Technol.* **2011**, *45*, 10605.
[9] W. Ouyang, S. Zheng, C. Wu, X. Hu, R. Chen, L. Zhuo, Z. Wang, *Int. J. Hydrogen Energy* **2021**, *46*, 32559.
[10] A. J. Rieth, Y. Tulchinsky, M. Dincă, *J. Am. Chem. Soc.* **2016**, *138*, 9401.
[11] K. Vikrant, V. Kumar, K. H. Kim, D. Kukkar, *J. Mater. Chem. A* **2017**, *5*, 22877.
[12] D. W. Kim, D. W. Kang, M. Kang, J. H. Lee, J. H. Choe, Y. S. Chae, D. S. Choi, H. Yun, C. S. Hong, *Angew. Chem., Int. Ed.* **2020**, *59*, 22531.
[13] M. K. Matikolaei, E. Binaeian, *ACS Appl. Mater. Interfaces* **2021**, *13*, 27159.
[14] L. Guo, J. Hurd, M. He, W. Lu, J. Li, D. Crawshaw, M. Fan, S. Sapchenko, Y. Chen, X. Zeng, M. Kippax-Jones, W. Huang, Z. Zhu, P. Manuel, M. D. Frogley, D. Lee, M. Schröder, S. Yang, *Commun. Chem* **2023**, *6*, 55.
[15] S. Wang, Y. Fu, T. Wang, W. Liu, J. Wang, P. Zhao, H. Ma, Y. Chen, P. Cheng, Z. Zhang, *Nat. Commun* **2023**, *14*, 7261.
[16] A. Takahashi, H. Tanaka, D. Parajuli, T. Nakamura, K. Minami, Y. Sugiyama, Y. Hakuta, S. Ohkoshi, T. Kawamoto, *J. Am. Chem. Soc.* **2016**, *138*, 6376.
[17] B. E. R. Snyder, A. B. Turkiewicz, H. Furukawa, M. V. Paley, E. O. Velasquez, M. N. Dods, J. R. Long, *Nature* **2023**, *613*, 287.

[18] P. Zhou, Z. Li, Z. Wang, H. Wang, Y. Zhao, J. Wang, *Sep. Purif. Technol* **2024**, *336*, 126348.
[19] J. R. Muralidhar, K. Salikolimi, K. Adachi, D. Hashizume, K. Kodama, T. Hirose, Y. Ito, M. Kawamoto, *J. Am. Chem. Soc* **2023**, *145*, 16973.
[20] B. Sakintuna, F. Lamari-Darkrim, M. Hirscher, *Int. J. Hydrogen Energy* **2007**, *32*, 1121.
[21] F. Marques, M. Balcerzak, F. Winkelmann, G. Zepon, M. Felderhoff, *Energy Environ. Sci.* **2021**, *14*, 5191.
[22] G. L. Bridger, M. L. Salutsky, R. W. Starostka, *J. Agric. Food Chem.* **1962**, *10*, 181.
[23] T. Kozawa, K. Fukuyama, A. Kondo, M. Naito, *ACS Omega* **2019**, *4*, 5690.
[24] T. Kozawa, K. Fukuyama, A. Kondo, M. Naito, *Mater. Res. Bull.* **2021**, *135*, 111149.
[25] A. Yuan, J. Wu, L. Bai, S. Ma, Z. Huang, Z. Tong, *J. Chem. Eng. Data* **2008**, *53*, 1066.
[26] R. L. Frost, *Spectrochim. Acta A Mol. Biomol. Spectrosc.* **2004**, *60*, 1439.
[27] J. Rodrigues, S. O. Pereira, J. Zanoni, B. P. Falcão, N. F. Santos, J. P. Moura, M. R. Soares, L. Rino, F. M. Costa, T. Monteiro, *Mater. Today Chem* **2022**, *23*, 100629.
[28] A. R. Kampf, X. Gu, H. Yang, C. Ma, J. Marty, *Mineral. Mag.* **2024**, *88*, 312.
[29] T. Kozawa, K. Fukuyama, K. Kushimoto, S. Ishihara, J. Kano, A. Kondo, M. Naito, *Sci. Rep.* **2021**, *11*, 210.
[30] S. Suzuki, T. Kozawa, T. Murakami, M. Naito, *Mater. Res. Bull.* **2017**, *90*, 218.
[31] W. T. A. Harrison, A. N. Sobolev, M. L. F. Phillips, *Acta Crystallogr.* **2001**, *57*, 508.
[32] A. Wei, X. W. Sun, C. X. Xu, Z. L. Dong, Y. Yang, S. T. Tan, W. Huang, *Nanotechnology* **2006**, *17*, 1740.
[33] Y. G. Zhang, Y. J. Zhu, F. Chen, T. W. Sun, Y. Y. Jiang, *CrystEngComm* **2017**, *19*, 1965.
[34] S. N. Le, A. Navrotsky, *J. Solid State Chem* **2008**, *181*, 20.
[35] Z. Amghouz, B. Ramajo, S. A. Khainakov, I. da Silva, G. R. Castro, J. R. García, S. García-Granda, *Chem. Commun* **2014**, *50*, 6729.
[36] X. Bu, P. Feng, T. E. Gier, G. D. Stucky, *Zeolites* **1997**, *19*, 200.
[37] K. Momma, F. Izumi, *J. Appl. Crystallogr.* **2011**, *44*, 1272.
[38] A. Choudhury, S. Natarajan, C. N. R. Rao, *Inorg. Chem* **2000**, *39*, 4295.
[39] C. N. R. Rao, S. Natarajan, A. Choudhury, S. Neeraj, A. A. Ayi, *Acc. Chem. Res.* **2001**, *34*, 80.
[40] S. Natarajan, S. Mandal, *Angew. Chem., Int. Ed.* **2008**, *47*, 4798.